TECHNISCHE UNIVERSITÄT CHEMNITZ

Jens Rückert Arnd Meyer

Kirchhoff Plates and Large Deformation

CSC/12-01

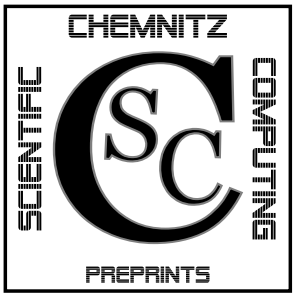

Chemnitz Scientific Computing Preprints

Impressum:

Chemnitz Scientific Computing Preprints — ISSN 1864-0087
(1995–2005: Preprintreihe des Chemnitzer SFB393)

Herausgeber:
Professuren für
Numerische und Angewandte Mathematik
an der Fakultät für Mathematik
der Technischen Universität Chemnitz

Postanschrift:
TU Chemnitz, Fakultät für Mathematik
09107 Chemnitz
Sitz:
Reichenhainer Str. 41, 09126 Chemnitz

`http://www.tu-chemnitz.de/mathematik/csc/`

TECHNISCHE UNIVERSITÄT CHEMNITZ

Chemnitz Scientific Computing Preprints

Jens Rückert Arnd Meyer

Kirchhoff Plates and Large Deformation

CSC/12-01

CSC/12-01 ISSN 1864-0087 April 2012

Contents

1 Introduction **1**

2 The $3D$-deformation energy **1**
2.1 General differential geometry in $3D$ 2
2.2 Deformation energy 3

3 Basic differential geometry of shells **5**
3.1 The initial mid surface 5
3.2 The initial shell 6
3.3 The plate as an exception of a shell 7

4 Kirchhoff assumption and the deformed plate **7**
4.1 Differential geometry of the deformed shell 7
4.2 The strain tensor of the deformed plate 8

5 Plate energy and boundary conditions **9**
5.1 The resulting Kirchhoff deformation energy 10
5.2 Boundary conditions 11

6 Numerical Example **12**
6.1 Plate deflection 12
6.2 Bending dominated plate deformation 15

Author's addresses:

Jens Rückert
Arnd Meyer
TU Chemnitz
Fakultät für Mathematik
D-09107 Chemnitz

`http://www.tu-chemnitz.de/mathematik/`

1 Introduction

In the simulation of deformations of plates it is well known that we have to use a special treatment of the thickness dependence. Therewith we achieve a reduction of dimension from $3D$ to $2D$.

For linear elasticity and small deformations several techniques are well established to handle the reduction of dimension and achieve acceptable numerical results. In the case of large deformations of plates with non-linear material behaviour there exist different problems. For example the analytical integration over the thickness of the plate is not possible due to the non-linearities arising from the material law and the large deformations themselves. There are several possibilities to introduce a hypothesis for the treatment of the plate thickness from the strong Kirchhoff assumption on one hand up to some hierarchical approaches on the other hand.

In this preprint we consider a model of using the Kirchhoff assumption. So first we give a short overview in useful differential geometry and explain the hypothesis mathematically.

The following section treats with the approximate solution of the PDE, we concern with. The preprint ends with some numerical examples.

2 The $3D$-deformation energy

In the entire paper we use the Einstein summation convention. Furthermore we understand a second order tensor as a pair of two vectors, for example $\boldsymbol{A}^1\boldsymbol{A}^2$ or similar. In general, it is any linear combination of such pairs. Accordingly tensors of higher order are built in the same manner. By the way we can consider a vector as a first order tensor.
Some calculation rules are defined for second order tensors. So the dot product maps the (3-dimensional) vector functions $\boldsymbol{U}$ onto vector functions again:

$$(\boldsymbol{A}^1\boldsymbol{A}^2)\cdot\boldsymbol{U} = \boldsymbol{A}^1(\boldsymbol{A}^2\cdot\boldsymbol{U})$$
$$\boldsymbol{U}\cdot(\boldsymbol{A}^1\boldsymbol{A}^2) = \boldsymbol{A}^2(\boldsymbol{A}^1\cdot\boldsymbol{U}).$$

The trace is defined as $tr(\boldsymbol{A}^1\boldsymbol{A}^2) = \boldsymbol{A}^1\cdot\boldsymbol{A}^2$ and the transposed tensor as $(\boldsymbol{A}^1\boldsymbol{A}^2)^\tau = \boldsymbol{A}^2\boldsymbol{A}^1$. The double dot product between two second order tensors is a scalar function. It is defined by

$$\boldsymbol{A}^1\boldsymbol{A}^2 : \boldsymbol{A}^3\boldsymbol{A}^4 = (\boldsymbol{A}^2\cdot\boldsymbol{A}^3)(\boldsymbol{A}^1\cdot\boldsymbol{A}^4).$$

Throughout this paper we display $2nd$ order tensors by gently rolled capital letters. Vectors are written in bold and matrices in underlined types. Therefor we

differ between the undeformed and the deformed configuration of the considered device by using capital and lower case letters, respectively.

Now, for the energy functional we restrict ourselves to nonlinear elastic material laws, where the stresses are nonlinear functions of strains.

2.1 General differential geometry in $3D$

We parametrize an undeformed domain in the Euclidean space as

$$\Omega_0 = \{\boldsymbol{X}(\eta) : \eta \in \mathcal{P} \subset \mathbb{R}^3\}$$

with $\eta = (\eta^1, \eta^2, \eta^3)$ a given curvilinear coordinate system. Then the η^i, $i = 1, 2, 3$, are the coordinates of the physical point $\boldsymbol{X}$ in the coordinate system η.

Now for every point in the domain Ω_0 with given coordinates (η^1, η^2, η^3) we denote the covariant tensor basis by

$$\boldsymbol{G}_i = \frac{\partial}{\partial \eta^i} \boldsymbol{X}, \quad i = 1, 2, 3 \tag{1}$$

and the contravariant tensor basis $\boldsymbol{G}^j$ by

$$\boldsymbol{G}_i \cdot \boldsymbol{G}^j = \delta_i^j, \quad i, j = 1, 2, 3.$$

The elements of

$$\underline{G} = (G_{ij})_{i,j=1}^3, \quad G_{ij} = \boldsymbol{G}_i \cdot \boldsymbol{G}_j, \tag{2}$$

are called the metric coefficients of the tensor basis.
With $G^{ij} = \boldsymbol{G}^i \cdot \boldsymbol{G}^j$,

$$\underline{G}^{-1} = \left(G^{ij}\right)_{i,j=1}^3$$

is true.

Then the volume element of the device is

$$dV = [\boldsymbol{G}_1, \boldsymbol{G}_2, \boldsymbol{G}_3]\, d\eta^1 d\eta^2 d\eta^3 = (det(\underline{G}))^{\frac{1}{2}}\ d\eta^1 d\eta^2 d\eta^3.$$

Furthermore, we define the gradient operator in the undeformed domain:

$$\text{Grad } = \boldsymbol{G}^i \frac{\partial}{\partial \eta^i}.$$

Now we depict a deformation of the device Ω_0 by a displacement vector $\boldsymbol{U}(\eta)$, defining an isomorphism

$$\omega : \Omega_0 \to \Omega_t, \qquad \boldsymbol{x}(\boldsymbol{U}) = \omega(\boldsymbol{X}) = \boldsymbol{X} + \boldsymbol{U}, \tag{3}$$

mapping every physical point $\boldsymbol{X}$ of the initial configuration to a physical point $\boldsymbol{x}$ of the deformed device Ω_t. Obviously, the deformed domain is parametrized as

$$\Omega_t = \{\boldsymbol{x}(\eta) : \boldsymbol{x}(\eta) = \boldsymbol{X}(\eta) + \boldsymbol{U}(\eta),\, \eta \in \mathcal{P}\}.$$

As before, we define the covariant and contravariant tensor basis as well as the gradient operator in Ω_t:

$$\begin{aligned} \boldsymbol{g}_i &= \frac{\partial}{\partial \eta^i}\boldsymbol{x}, \qquad i = 1,2,3 \\ \Rightarrow \exists \boldsymbol{g^i} :\ \boldsymbol{g}_i \cdot \boldsymbol{g}^j &= \delta_i^j, \qquad i,j = 1,2,3 \text{ and} \\ \operatorname{grad} &= \boldsymbol{g}^i \frac{\partial}{\partial \eta^i}. \end{aligned}$$

With the isomorphism (3) the second order tensor

$$\mathcal{F} = (\operatorname{Grad}\omega)^\tau$$

describes the deformation gradient. It can be shown that we can depict it by

$$\mathcal{F} = \boldsymbol{g}_i \boldsymbol{G}^i.$$

Then with the right Cauchy-Green deformation tensor

$$\mathcal{C} = \mathcal{F}^\tau \cdot \mathcal{F} \tag{4}$$

we define the strain tensor

$$\begin{aligned} \mathcal{E} &= \tfrac{1}{2}(\mathcal{C} - \mathcal{I}) \\ &= \operatorname{Grad}\boldsymbol{U} + (\operatorname{Grad}\boldsymbol{U})^\tau + \operatorname{Grad}\boldsymbol{U} \cdot (\operatorname{Grad}\boldsymbol{U})^\tau, \end{aligned} \tag{5}$$

where $\mathcal{I}$ is the unity tensor (the $2nd$-order tensor, mapping a vector onto itself).

2.2 Deformation energy

We define the deformation energy as

$$\varphi(\boldsymbol{U}) = \int_{\Omega_0} \psi(\boldsymbol{U})\, dV - f(\boldsymbol{U}). \tag{6}$$

Here, the linear functional f contains the volume and boundary forces, independent of $\boldsymbol{U}$. ψ is the energy density and depends on the three invariants of the right Cauchy-Green tensor. So with the acronyms

$$a_k = \frac{1}{k} tr(\mathcal{C})^k, \quad k = 1,2,3 \tag{7}$$

these invariants are

$$\begin{aligned} I_{\mathcal{C}} &= a_1 \\ II_{\mathcal{C}} &= \frac{1}{2}(a_1)^2 - a_2 \quad \text{and} \\ III_{\mathcal{C}} &= \frac{a_1^3 - 6a_1a_2 + 6a_3}{6} = det(\mathcal{C}). \end{aligned}$$

As most simple example we may use the neo-Hooke material, defined by its energy density

$$\psi(a_1, a_2, a_3) = \frac{\mu}{2}\left(a_1 - ln(III_{\mathcal{C}}) - 3\right) + \frac{K}{8} ln^2\left(III_{\mathcal{C}}\right),$$

where μ and the bulk modulus K depend on the material.

Now, $\boldsymbol{U}$ minimizes φ. So for all virtuell displacement vectors $\boldsymbol{V}$ of appropriate function spaces we have

$$\varphi'(\boldsymbol{U}; \boldsymbol{V}) = \int_{\Omega_0} \psi'(\boldsymbol{U}; \boldsymbol{V})\, dV - f(\boldsymbol{V}) \stackrel{!}{=} 0.$$

Therefore $\varphi'(\boldsymbol{U}; \boldsymbol{V})$ is a linear functional over $\boldsymbol{V}$, where

$$\psi'(\boldsymbol{U}; \boldsymbol{V}) = \sum_{k=1}^{3} \frac{\partial \psi}{\partial a_k} \left(\frac{\partial a_k}{\partial \mathcal{C}}\right) : \mathcal{C}'(\boldsymbol{U}; \boldsymbol{V}).$$

With (5)

$$\begin{aligned} \mathcal{C}'(\boldsymbol{U}; \boldsymbol{V}) &= 2\mathcal{E}'(\boldsymbol{U}; \boldsymbol{V}) \\ &= \operatorname{Grad} \boldsymbol{V} + \operatorname{Grad} \boldsymbol{V}^{\tau} + \operatorname{Grad} \boldsymbol{U} \cdot \operatorname{Grad} \boldsymbol{V}^{\tau} + \operatorname{Grad} \boldsymbol{V} \cdot \operatorname{Grad} \boldsymbol{U}^{\tau}, \end{aligned}$$

consistently. The derivatives of the a_k with respect to the tensor $\mathcal{C}$ are easily calculated from (7) as $\frac{\partial a_k}{\partial \mathcal{C}} = \mathcal{C}^{k-1}(\boldsymbol{U})$. Therefore

$$\psi'(\boldsymbol{U}; \boldsymbol{V}) = \sum_{k=1}^{3} 2\frac{\partial \psi}{\partial a_k} \left(\mathcal{C}^{k-1} : \mathcal{E}'(\boldsymbol{U}; \boldsymbol{V})\right),$$

and the second order tensor

$$\overset{2}{T}(\boldsymbol{U}) := 2\sum_{k=1}^{3} \frac{\partial \psi}{\partial a_k} \mathcal{C}^{k-1}(\boldsymbol{U}) \tag{8}$$

is the well-known second Piola-Kirchhoff stress tensor, as can be derived from the approach of the equilibrium of forces, as well.

With the abbreviation $a(\boldsymbol{U};\boldsymbol{V}) := \int_{\Omega_0} \overset{2}{\mathcal{T}}(\boldsymbol{U}) : \mathcal{E}'(\boldsymbol{U},\boldsymbol{V})\, dV$ our weak formulation is:

Solve for the vector function $\boldsymbol{U} \in (\mathbb{H}_0^1(\Omega_0))^3$

$$a(\boldsymbol{U};\boldsymbol{V}) = f(\boldsymbol{V})\ \forall \boldsymbol{V} \in (\mathbb{H}_0^1(\Omega_0))^3. \tag{9}$$

Here,

$$(\mathbb{H}_0^1(\Omega_0))^3 := \{\boldsymbol{U} \in (\mathbb{H}^1(\Omega_0))^3 : \boldsymbol{U} = \boldsymbol{0}\, \forall \boldsymbol{X}(\eta^1,\eta^2,\eta^3) \in \Gamma_D \subset \partial\Omega_0\},$$

denotes the vector valued Sobolev space with homogeneous Dirichlet boundary conditions on Γ_D, the Dirichlet boundary part of $\partial\Omega_0$.

This problem leads to a set of non-linear equations. For solving this, we use Newton's method. Therefor we need the second derivative of the energy functional

$$\varphi''(\boldsymbol{U};\boldsymbol{\delta U},\boldsymbol{V}) = \int_{\Omega_0} \overset{2}{\mathcal{T}}'(\boldsymbol{U};\boldsymbol{\delta U}) : \mathcal{E}'(\boldsymbol{U};\boldsymbol{V}) + \overset{2}{\mathcal{T}}(\boldsymbol{U}) : \mathcal{E}''(\boldsymbol{U};\boldsymbol{\delta U},\boldsymbol{V})\, d\Omega_0.$$

3 Basic differential geometry of shells

To describe large deformations with shell theory, which combines aspects of continuum mechanics and differential geometry, it is used to work with both, matrices and tensors. So, we use tensors to discribe the differential geometry and switch to matrix syntax to make up the weak formulation. We begin with the differential geometry of shells in general. Later on, we consider the initial configuration as a plane shell, called plate.
In what follows all indices now run between 1 and 2.

3.1 The initial mid surface

In this paragraph we discribe the basic theory of the differential geometry on the undeformed shell, the initial domain. In the inital configuration all vectors and matrices, mainly the co- and contravariant basis vectors and the matrices of the first and the second fundamental forms, are typed in capital letters.

As midsurface of the undeformed shell we consider

$$\Omega_0^m := \{\boldsymbol{Y}(\eta^1,\eta^2) : (\eta^1,\eta^2) \in \mathcal{P}_2 \subset \mathbb{R}^2\} \subset \mathbb{R}^3. \tag{10}$$

Here, $\boldsymbol{Y}$ denote the points of the surface in the 3-dimensional space and the coordinates (η^1,η^2) run throughout the parameter domain $\mathcal{P}_2$. Therewith we get

the tangential vectors

$$\boldsymbol{A}_i = \frac{\partial}{\partial \eta^i}\boldsymbol{Y}, \quad i = 1,2, \qquad \text{and the surface normal vector}$$
$$\boldsymbol{A}_3 = \boldsymbol{A}^3 = \frac{\boldsymbol{A}_1 \times \boldsymbol{A}_2}{|\boldsymbol{A}_1 \times \boldsymbol{A}_2|}, \tag{11}$$

which define a covariant tensor basis in $\mathbb{R}^3$.

The first fundamental forms, calculated in this covariant tensor basis, are written as (2×2) matrices:

$$\underline{A} = (A_{ij})_{i,j=1}^2, \quad A_{ij} = \boldsymbol{A}_i \cdot \boldsymbol{A}_j, \quad \text{and the second fundamental forms}$$
$$\underline{B} = (B_{ij})_{i,j=1}^2, \quad B_{ij} = \left(\frac{\partial^2}{\partial \eta^i \partial \eta^j}\boldsymbol{Y}\right) \cdot \boldsymbol{A}_3 = \boldsymbol{A}_{i,j} \cdot \boldsymbol{A}_3 = -\boldsymbol{A}_i \cdot \boldsymbol{A}_{3,j}, \text{ respectively.}$$

We define the corresponding contravariant tensor basis from

$$\boldsymbol{A}^j = A^{jk}\boldsymbol{A}_k \quad \text{with} \quad \boldsymbol{A}^j \cdot \boldsymbol{A}_k = \delta_k^j, \text{ where } A^{jk} \text{ are the entries of } \underline{A}^{-1},$$

and the surface element by

$$d\mathcal{S} = |\boldsymbol{A}_1 \times \boldsymbol{A}_2|\, d\eta^1 d\eta^2 = (det\underline{A})^{\frac{1}{2}}\, d\eta^1 d\eta^2.$$

Now the gradient operator on the tangential space, the surface gradient, is specified by

$$\text{Grad}_S = \boldsymbol{A}^i \frac{\partial}{\partial \eta^i}.$$

3.2 The initial shell

We understand the initial shell as a 3-dimensional manifold

$$\Omega_0 := \left\{ \boldsymbol{X}(\eta^1, \eta^2, \tau = \eta^3) = \boldsymbol{Y}(\eta^1, \eta^2) + h\tau \boldsymbol{A}_3,\ (\eta^1, \eta^2) \in \mathcal{P}_2, |\tau| < \frac{1}{2} \right\}$$

with constant thickness h and $\boldsymbol{A}_3$ from (11). Without loss of generality we use $\tau = \eta^3$ as a synonym for the thickness coordinate and consider the coordinates η^i, $i = 1,2$, providing the lengths of dimensions in the according directions. Then the $\boldsymbol{A}_i$ and $\boldsymbol{A}^i$, $i = 1,2$ have to be dimensionless, consistently. Meanwhile $\boldsymbol{A}_3 = \boldsymbol{A}^3$ has no dimension, anyway. The covariant tensor basis (1) from 2.1 is now specified by

$$\boldsymbol{G}_i = \frac{\partial}{\partial \eta^i}\boldsymbol{X} = \boldsymbol{A}_i + h\tau \boldsymbol{A}_{3,i} \quad i = 1,2 \text{ and} \tag{12}$$
$$\boldsymbol{G}_3 = h\boldsymbol{A}_3$$

as well as the contravariant tensor basis $\boldsymbol{G}^i,\ i=1,2$ and $\boldsymbol{G}^3 = h^{-1}\boldsymbol{A}_3$.

Then the matrix of the metric coefficients (2) is calculable.

Obviously, $det(\underline{G}) = h^2\, det(\widehat{\underline{G}})$ with the (2×2)-matrix

$$\begin{aligned}\widehat{\underline{G}} &= (G_{ij})_{i,j=1}^2, \quad G_{ij} = \boldsymbol{G}_i \cdot \boldsymbol{G}_j \\ &= \underline{A}(\underline{I} - h\tau\underline{A}^{-1}\underline{B})^2 = (\underline{A} - h\tau\underline{B})\underline{A}^{-1}(\underline{A} - h\tau\underline{B}).\end{aligned} \tag{13}$$

Hence, the volume element of the shell is

$$dV = [\boldsymbol{G}_1, \boldsymbol{G}_2, \boldsymbol{G}_3]\, d\eta^1 d\eta^2 d\tau = h\, \det(\widehat{\underline{G}})^{\frac{1}{2}}\, d\eta^1 d\eta^2 d\tau.$$

3.3 The plate as an exception of a shell

Here, on the midsurface Ω_0^m in (10) we have the simplification that the physical points $\boldsymbol{Y}$ are in the $\boldsymbol{e}_1$ - $\boldsymbol{e}_2$ - plane, for instance

$$\boldsymbol{Y}(\eta^1, \eta^2) = \boldsymbol{e}_1 \cdot \eta^1 + \boldsymbol{e}_2 \cdot \eta^2,$$

where the $\eta^i,\ i=1,2$ feature the length of the dimension in direction of each unit vector $\boldsymbol{e}_i,\ i=1,2$. This simplification yields $\boldsymbol{A}_3 = \boldsymbol{e}_3$, independent of (η^1, η^2). From this we have

$$\boldsymbol{G}_i = \boldsymbol{e}_i, \quad \boldsymbol{G}_3 = h\boldsymbol{e}_3 \quad \text{and} \quad \underline{B} = \mathbb{O}\,.$$

4 Kirchhoff assumption and the deformed plate

4.1 Differential geometry of the deformed shell

The following assumption is one possibility to reduce the space dimension. The idea is to discribe the deformed shell by its midsurface only. Therefore we do not allow any change in thickness of the shell and assume it to be shear rigid. This means that a certain straight fibre of points

$$\left\{\boldsymbol{Y}(\eta^1, \eta^2) + h\tau\boldsymbol{A}_3(\eta^1, \eta^2) : |\tau| \le \frac{1}{2}\right\},$$

which is perpendicular to the undeformed midsurface Ω_0^m (10), has to be straight and perpendicular to the deformed midsurface

$$\Omega_t^m = \left\{\boldsymbol{y}(\eta_1, \eta_2) = \boldsymbol{Y}(\eta^1, \eta^2) + \boldsymbol{U}(\eta^1, \eta^2) : (\eta^1, \eta^2) \in \mathcal{P}_2\right\} \tag{14}$$

after deformation, as well. Here, $\boldsymbol{U}$ is the unknown displacement vector (a function of (η^1, η^2) as well as of $\boldsymbol{Y}$).
The Kirchhoff assumption defines the deformed shell as

$$\Omega_t = \left\{ \boldsymbol{x}(\eta^1, \eta^2, \tau) = \boldsymbol{y}(\eta^1, \eta^2) + h\tau \boldsymbol{a}_3 \right\}, \tag{15}$$

where $\boldsymbol{a}_3$ is the new surface normal vector of the deformed midsurface Ω_t^m following its differential geometry:
With

$$\boldsymbol{a}_i = \frac{\partial}{\partial \eta^i} \boldsymbol{y} = \boldsymbol{A}_i + \boldsymbol{U}_{,i}$$

the tangential vectors after deformation, we have

$$\boldsymbol{a}_3 = \frac{\boldsymbol{a}_1 \times \boldsymbol{a}_2}{|\boldsymbol{a}_1 \times \boldsymbol{a}_2|} \tag{16}$$

as surface normal vector of Ω_t^m. Consequently we get

$$\begin{aligned} \underline{a} &= (a_{ij})_{i,j=1}^2 \quad \text{with} \quad a_{ij} = \boldsymbol{a}_i \cdot \boldsymbol{a}_j \\ \underline{b} &= (b_{ij})_{i,j=1}^2 \quad \text{with} \quad b_{ij} = \boldsymbol{a}_{i,j} \cdot \boldsymbol{a}_3 \end{aligned}$$

the new first and second fundamental forms.
Now the $3D$ covariant basis is

$$\begin{aligned} \boldsymbol{g}_i &= \frac{\partial}{\partial \eta^i} \boldsymbol{x} = \boldsymbol{a}_i + h\tau \boldsymbol{a}_{3,i} = \boldsymbol{A}_i + \boldsymbol{U}_{,i} + h\tau \boldsymbol{a}_{3,i}, \quad i = 1, 2 \\ \boldsymbol{g}_3 &= h\boldsymbol{a}_3. \end{aligned} \tag{17}$$

Analogously to $\widehat{\underline{G}}$ in (13) we can define the (2×2)-matrix $\widehat{\underline{g}} = (g_{ij})_{i,j=1}^2$ with $g_{ij} = \boldsymbol{g}_i \cdot \boldsymbol{g}_j$, yielding

$$\widehat{\underline{g}} = \underline{a}(\underline{I} - h\tau \underline{a}^{-1} \underline{b})^2 = (\underline{a} - h\tau \underline{b}) \underline{a}^{-1} (\underline{a} - h\tau \underline{b}).$$

Hence, with (14) and (15) the new $3D$-deformation vector is

$$\boldsymbol{U}^{3D}(\eta^1, \eta^2, \tau) = \boldsymbol{U} + h\tau(\boldsymbol{a}_3(\boldsymbol{U}) - \boldsymbol{e}_3), \tag{18}$$

with the vector field $\boldsymbol{U}$, depending on (η^1, η^2) only.

4.2 The strain tensor of the deformed plate

We deduce the $3D$ deformation gradient from (12, 17) in relation with 3.3 as

$$\begin{aligned} \mathcal{F} &= \boldsymbol{g}_i \boldsymbol{G}^i + \boldsymbol{a}_3 \boldsymbol{A}^3 \\ &= (\boldsymbol{a}_1 + h\tau \boldsymbol{a}_{3,1}) \boldsymbol{e}_1 + (\boldsymbol{a}_2 + h\tau \boldsymbol{a}_{3,2}) \boldsymbol{e}_2 + \boldsymbol{a}_3 \boldsymbol{e}_3. \end{aligned}$$

Then, the coefficients of the right Cauchy Green deformation tensor (4) are given in

$$\mathcal{C} = \mathcal{F}^\tau \cdot \mathcal{F} = c_{ij}\boldsymbol{e}_i\boldsymbol{e}_j + \boldsymbol{e}_3\boldsymbol{e}_3 \tag{19}$$

$$\text{with} \quad c_{ij} = (\boldsymbol{a}_i + h\tau\boldsymbol{a}_{3,i}) \cdot (\boldsymbol{a}_j + h\tau\boldsymbol{a}_{3,j}), \quad i = 1, 2. \tag{20}$$

So, with (5) we get the $3D$-strain tensor of the plate as

$$\mathcal{E} = \varepsilon_{ij}\boldsymbol{e}_i\boldsymbol{e}_j \tag{21}$$

$$\text{with} \quad 2\varepsilon_{ij} = (\boldsymbol{a}_i + h\tau\boldsymbol{a}_{3,i}) \cdot (\boldsymbol{a}_j + h\tau\boldsymbol{a}_{3,j}), \quad i = 1, 2. \tag{22}$$

For using matrix syntax we define the matrices, containing the coefficients of the associated tensors in the chosen tensor base.

In case of the right Cauchy Green deformation tensor $\mathcal{C}$, given in (19,20), the appropriate matrix is

$$\underline{c} = (c_{ij})_{i,j=1}^2. \tag{23}$$

With the help of the Gauß- and Weingarten equations and some mathematical transformations we obtain the submatrix

$$\underline{c} = (\underline{a} - h\tau\underline{b})\underline{a}^{-1}(\underline{a} - h\tau\underline{b}) = \widehat{\underline{g}}. \tag{24}$$

Analogously, the matrix with the coefficients of the strain tensor (22) is

$$\underline{e} = (\varepsilon_{ij})_{i,j=1}^2$$

and

$$2\underline{e} = (\underline{a} - h\tau\underline{b})\underline{a}^{-1}(\underline{a} - h\tau\underline{b}) - \underline{I}.$$

5 Plate energy and boundary conditions

In this section we consider $\boldsymbol{U}^{3D}$, defined in (18), with $\boldsymbol{U} \in \mathbb{H}^{KH}$, where

$$\mathbb{H}^{KH} := \{\mathbb{H}^2(\Omega_0^m) \text{ with appropriate boundary conditions}\} \tag{25}$$

is a special function space, due to the Kirchhoff assumption. Its boundary conditions are considered in 5.2.

5.1 The resulting Kirchhoff deformation energy

We consider the energy functional (6) but use $\boldsymbol{U}^{3D}$ from (18). Then

$$\varphi(\boldsymbol{U}^{3D}) = \varphi\left(\boldsymbol{U} + h\tau(\boldsymbol{a}_3(\boldsymbol{U}) - \boldsymbol{e}_3)\right) = \int_{\Omega_0} \psi(\boldsymbol{U}^{3D})\, dV - f(\boldsymbol{U}^{3D}) \tag{26}$$
$$=: \widehat{\varphi}(\boldsymbol{U}) = \int_{\Omega_0} \widehat{\psi}(\boldsymbol{U})\, dV - f(\boldsymbol{U}) \quad \text{with } \boldsymbol{U} \in \mathbb{H}^{KH}.$$

Analogously to the real $3D$-deformation vector $\boldsymbol{U}$ in 2.2, that minimizes the energy functional (6), the new $\boldsymbol{U}(\eta^1, \eta^2)$, here, minimizes the energy functional $\widehat{\varphi}$ above, such that $\boldsymbol{U}^{3D}$ minimizes the deformation energy (2.2) over a nonlinear set (18). Hence, the first derivative $\widehat{\varphi}'(\boldsymbol{U}; \boldsymbol{V})$ should vanish for all virtuell displacements $\boldsymbol{V} \in \mathbb{H}^{KH}$:

$$\widehat{\varphi}'(\boldsymbol{U}; \boldsymbol{V}) \stackrel{!}{=} 0.$$

The derivative of this energy functional arises from the variation of $\widehat{\psi}$,

$$\widehat{\psi}(\boldsymbol{U} + \boldsymbol{V}) = \widehat{\psi}(\boldsymbol{U}) + \widehat{\psi}'(\boldsymbol{U}; \boldsymbol{V}) + \text{ h.o.t. }.$$

Hence,

$$\widehat{\psi}'(\boldsymbol{U}, \boldsymbol{V}) = \frac{\partial \psi(\boldsymbol{U}^{3D})}{\partial \boldsymbol{U}(\eta^1, \eta^2)} \circ \boldsymbol{V}$$
$$= \overset{2}{T}(\boldsymbol{U}^{3D}) : \mathcal{E}'\left(\boldsymbol{U}^{3D}; \mathcal{L}(\boldsymbol{V})\right),$$

with

$$\mathcal{L}(\boldsymbol{V}) := \frac{\partial \boldsymbol{U}^{3D}}{\partial \boldsymbol{U}} \circ \boldsymbol{V},$$

a linear operator w.r.t. $\boldsymbol{V}$ arising from the variation of $\boldsymbol{U}^{3D}$,

$$\boldsymbol{U}^{3D}(\boldsymbol{U} + \boldsymbol{V}) = \boldsymbol{U}^{3D}(\boldsymbol{U}) + \mathcal{L}(\boldsymbol{V}) + \text{ h.o.t. }.$$

Obviously,

$$\mathcal{L}(\boldsymbol{V}) = \boldsymbol{V} + h\tau \boldsymbol{a}_3(\boldsymbol{U}; \boldsymbol{V}) \tag{27}$$

with $\boldsymbol{a}_3(\boldsymbol{U}; \boldsymbol{V})$ a differential operator, which can be retrieved from the variation of $\boldsymbol{a}_3$:

$$\boldsymbol{a}_3(\boldsymbol{U} + \boldsymbol{V}) = \boldsymbol{a}_3(\boldsymbol{U}) + \boldsymbol{a}_3(\boldsymbol{U}; \boldsymbol{V}) + \text{ h.o.t. }.$$

Due to the Kirchhoff assumption, we have seen, that, in comparison to the $3D$-deformation energy in 2.2, we have to accomplish a further linear operator $\mathcal{L}$,

including a differential operator $\boldsymbol{a}_3(\boldsymbol{U};\boldsymbol{V}) = \left(\frac{\partial \boldsymbol{a}_3}{\partial \boldsymbol{U}}\right) \circ \boldsymbol{V}$, applied to virtuell displacements $\boldsymbol{V}$ from an appropriate function space $\mathbb{H}^{KH}$.

Now, with

$$a(\boldsymbol{U};\boldsymbol{V}) = \int_{\Omega_0} \overset{2}{T}(\boldsymbol{U}^{3D}) : \mathcal{E}'(\boldsymbol{U}^{3D};\mathcal{L}(\boldsymbol{V}))\, dV \tag{28}$$

we can formulate the new weak formulation:

Find the solution $\boldsymbol{U} \in \mathbb{H}^{KH}$ such that

$$a(\boldsymbol{U};\boldsymbol{V}) = f(\boldsymbol{V}) \text{ for all } \boldsymbol{V} \in \mathbb{H}^{KH}. \tag{29}$$

Until now, we have not considered any boundary conditions of our function space $\mathbb{H}^{KH}$. Therefore we take a closer look to this space in the following paragraph.

5.2 Boundary conditions

As easily seen in (18), $\boldsymbol{U}^{3D}$ contains the normal of the deformed midsurface, $\boldsymbol{a}_3$, which is a nonlinear differential operator, applied to $\boldsymbol{U}$. In (28) differential operators are applied to $\boldsymbol{U}^{3D}$ and therefore to $\boldsymbol{a}_3$, consistently. Hence, we need the second partial derivatives in $\boldsymbol{U}$ and $\mathbb{H}^{KH}(\Omega_0^m) \subset (\mathbb{H}^2(\Omega_0^m))^3$, as subspace of the Sobolev function space in (25), is motivated.

We consider the normal $\boldsymbol{a}_3$ in (16) at the boundary of the plate. Hence, one of the coordinates (η^1, η^2) has to be constant. W.l.o.g. we consider $\eta^1 = constant$, defining a boundary part (for all η^2 and for all $\tau \in \left[-\frac{1}{2}, \frac{1}{2}\right]$). If this boundary part is classified as hard clamped with homogeneous boundary conditions, then $\boldsymbol{U} = \boldsymbol{0}$ and $\boldsymbol{a}_3 = \boldsymbol{e}_3$ as simply seen in (14) and (15). Generalized inhomogeneous boundary conditions mean $\boldsymbol{U}$ and $\boldsymbol{a}_3$ are appropriately given. Now we evolute the contained crossproduct, intercepting higher order parts of $\boldsymbol{U}$.

$$\begin{aligned}
\boldsymbol{a}_3 = \frac{\boldsymbol{a}_1 \times \boldsymbol{a}_2}{|\boldsymbol{a}_1 \times \boldsymbol{a}_2|} &= \frac{(\boldsymbol{e}_1 + \boldsymbol{U}_{,1}) \times (\boldsymbol{e}_2 + \boldsymbol{U}_{,2})}{|(\boldsymbol{e}_1 + \boldsymbol{U}_{,1}) \times (\boldsymbol{e}_2 + \boldsymbol{U}_{,2})|} \\
\iff \qquad (\boldsymbol{e}_1 + \boldsymbol{U}_{,1}) \times (\boldsymbol{e}_2 + \boldsymbol{U}_{,2}) &= \boldsymbol{a}_3\, |(\boldsymbol{e}_1 + \boldsymbol{U}_{,1}) \times (\boldsymbol{e}_2 + \boldsymbol{U}_{,2})| \\
\iff \quad \boldsymbol{e}_3 + (\boldsymbol{e}_1 \times \boldsymbol{U}_{,2}) + (\boldsymbol{U}_{,1} \times \boldsymbol{e}_2) &= \boldsymbol{a}_3 |\boldsymbol{e}_3 + (\boldsymbol{e}_1 \times \boldsymbol{U}_{,2}) + (\boldsymbol{U}_{,1} \times \boldsymbol{e}_2)| \\
\iff \quad \boldsymbol{e}_3 + (\boldsymbol{e}_1 \times \boldsymbol{U}_{,2}) - (\boldsymbol{e}_2 \times \boldsymbol{U}_{,1}) &= \boldsymbol{a}_3\, |\boldsymbol{e}_3 + (\boldsymbol{e}_1 \times \boldsymbol{U}_{,2}) - (\boldsymbol{e}_2 \times \boldsymbol{U}_{,1})|
\end{aligned}$$

For a hard clamped boundary part the condition $\boldsymbol{a}_3 = \boldsymbol{e}_3$ means

$$\begin{pmatrix} U^{(3)}_{,1} \\ -U^{(3)}_{,2} \\ 1 + U^{(2)}_{,2} + U^{(1)}_{,1} \end{pmatrix} = \left| \begin{pmatrix} U^{(3)}_{,1} \\ -U^{(3)}_{,2} \\ 1 + U^{(2)}_{,2} + U^{(1)}_{,1} \end{pmatrix} \right| \begin{pmatrix} 0 \\ 0 \\ 1 \end{pmatrix}. \tag{30}$$

Hence,

$$U^{(3)}_{,1} = U^{(3)}_{,2} = 0$$

is the resulting boundary condition for the deformation vector.

In the case of soft clamping of the considered boundary part one of the two partial derivatives is free.

6 Numerical Example

6.1 Plate deflection

We consider the midsurface $\boldsymbol{Y}(\eta^1, \eta^2) = [0, 4] \times [0, 4] \times 0$ of a plate with a given thickness $h = 0.05$. The coarse triangulation consists of 4×4 uniform quadratic finite elements. All sites of the plate are hard clamped. We use a constant force $f = (0, 0, 1)^T$, which is applied in 5 incremental equidistant steps on the starting coarse mesh, followed by 5 times uniform mesh refinement together with the Newton iteration on each refinement step. Figure 1 displays the norm of the strain tensor at the midsurface for the initial mesh with 16 elements (1a) and after all refinements with 16.384 elements (1b).

During the incremental stage we achieve a mean value of about 13 iterations in the PCG method per Newton step. Here we use a special hierachical preconditioner, especially adopted to the Bogner-Fox-Schmidt elements. The mean value of Newton steps during this stage is between 3 and 4. Throughout the mesh refinement the PCG needs about 65 iterations per Newton step for again 3 to 4 Newton steps on each mesh. As stopping criterion for the Newton's method we recommand $\frac{\|\delta u\|}{\|u\|} \leq 10^{-5}$.

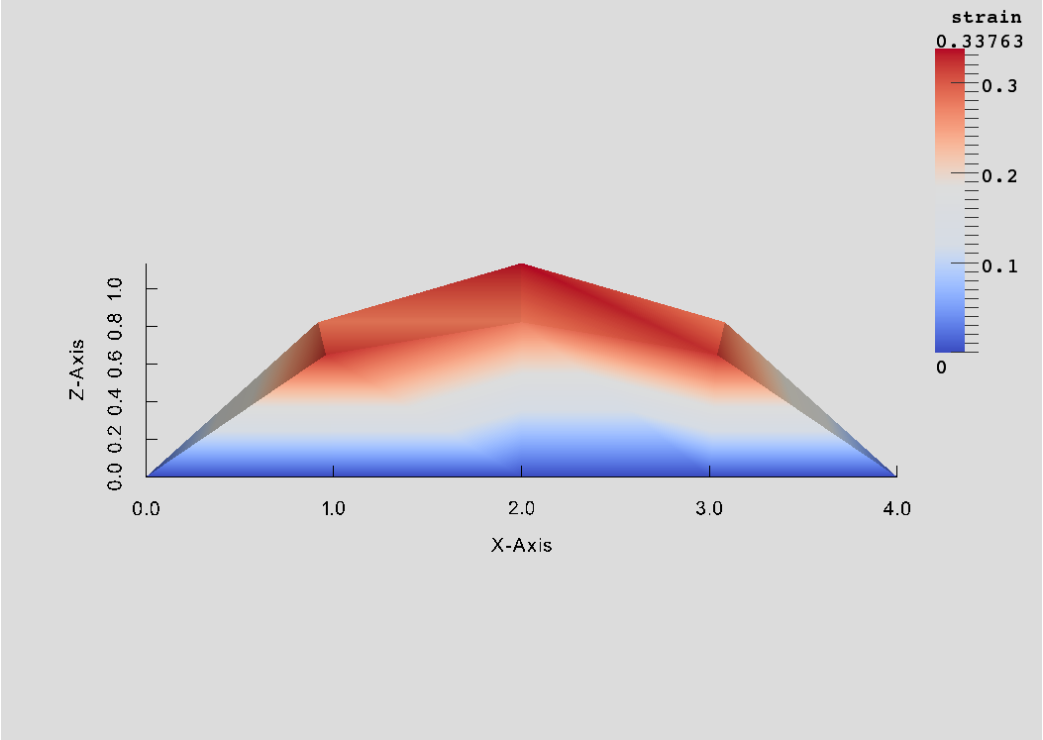

(a) 16 elements.

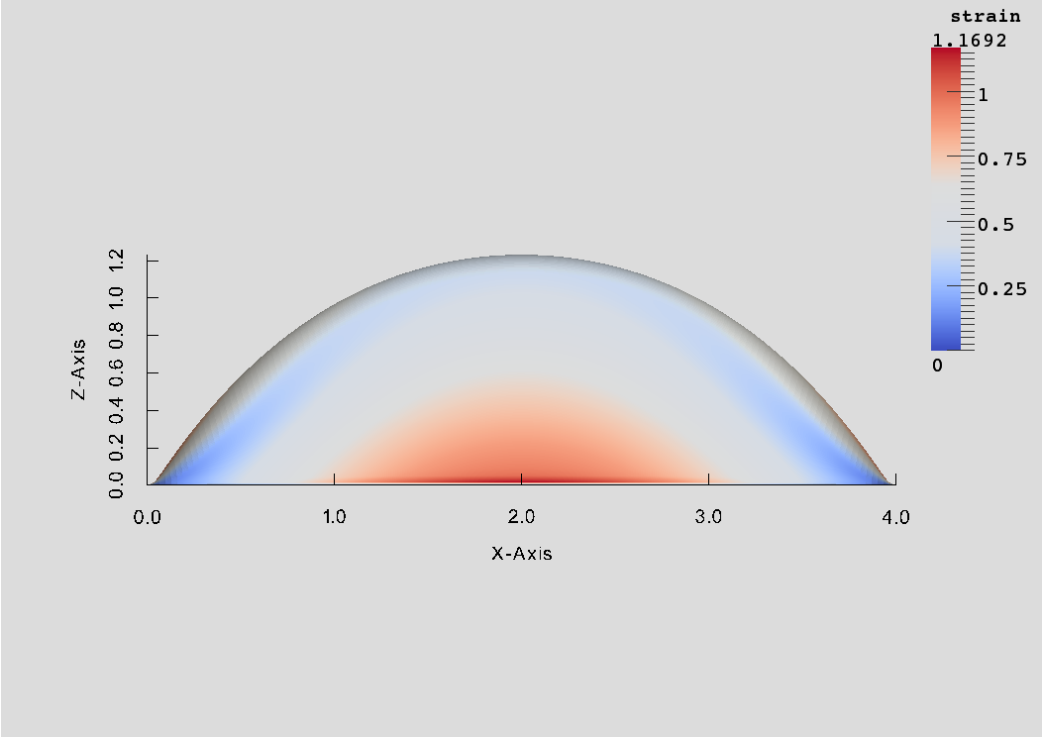

(b) 16384 elements.

Figure 1: Norm of the strain tensor at $\tau = 0$.

In table 1 we now consider the elements of the displacement vector $\boldsymbol{U}$ and the norm of strain tensor in the four points $P1(1,1)$, $P2(1,2)$, $P3(2,2)$ and $P4(2,1)$ in every refinement state. Figure 2 shows the position of the four points in the midsurface of the undeformed plate.

$\#El$		16	64	256	1024	4096	16384
$P1$	$U^{(1)}$	-4.2E-02	-4.8E-02	-5.1E-02	-5.2E-02	-5.2E-02	-5.2E-02
	$U^{(2)}$	-4.2E-02	-4.8E-02	-5.1E-02	-5.2E-02	-5.2E-02	-5.2E-02
	$U^{(3)}$	6.5E-01	6.8E-01	7.0E-01	7.2E-01	7.2E-01	7.2E-01
	$\|E\|_F$	3.2E-01	3.2E-01	3.5E-01	3.5E-01	3.5E-01	3.5E-01
$P2$	$U^{(1)}$	-8.3E-02	-8.5E-02	-8.8E-02	-8.9E-02	-8.9E-02	-8.9E-02
	$U^{(2)}$	1.1E-06	3.4E-07	5.5E-09	-8.8E-08	2.6E-08	3.4E-08
	$U^{(3)}$	8.2E-01	8.6E-01	8.9E-01	9.1E-01	9.1E-01	9.1E-01
	$\|E\|_F$	2.8E-01	4.3E-01	4.7E-01	4.6E-01	4.6E-01	4.6E-01
$P3$	$U^{(1)}$	7.9E-07	-1.9E-07	4.4E-08	-8.6E-08	-9.1E-10	-3.1E-08
	$U^{(2)}$	1.4E-06	2.7E-07	5.5E-08	3.3E-08	-1.2E-08	-1.5E-08
	$U^{(3)}$	1.1395	1.1848	1.2130	1.2251	1.2294	1.2319
	$\|E\|_F$	3.4E-01	3.6E-01	3.7E-01	3.7E-01	3.7E-01	3.7E-01
$P4$	$U^{(1)}$	4.2E-07	-1.6E-07	-1.2E-07	-5.5E-08	-3.2E-08	-2.9E-08
	$U^{(2)}$	-8.3E-02	-8.5E-02	-8.8E-02	-8.9E-02	-8.9E-02	-8.9E-02
	$U^{(3)}$	8.2E-01	8.6E-01	8.9E-01	9.1E-01	9.1E-01	9.1E-01
	$\|E\|_F$	2.8E-01	4.3E-01	4.7E-01	4.6E-01	4.6E-01	4.6E-01

Table 1: Displacement vector and the norm of the strain tensor in $P1$ till $P4$.

In case of a linear elastic model the first two components of $\boldsymbol{U}$ would vanish completely. Hence, $U^{(1)}$ and $U^{(2)}$ in $P1$, $P2$ and $P4$ reflect the non-linearity. (In $P3$ we have $U^{(1)} = U^{(2)} = 0$ from the symmetry of the domain.)

In $P1$ the components of the displacement vector in direction of η^1 and η^2 are the same, due to inherent symmetries.

The component of the displacement vector in η^2-direction of $P4$ is the same as the component in η^1-direction of $P2$. The third components of the displacement

vectors are the same in both points as are the values for the strain tensors, due to the plate symmetry and the manner of deformation.

Obviously the third component of the displacement vector reaches its maximum over all nodes in $P3$, because this is the midpoint of the midsurface, as you can see in the pictures 1 and 2.

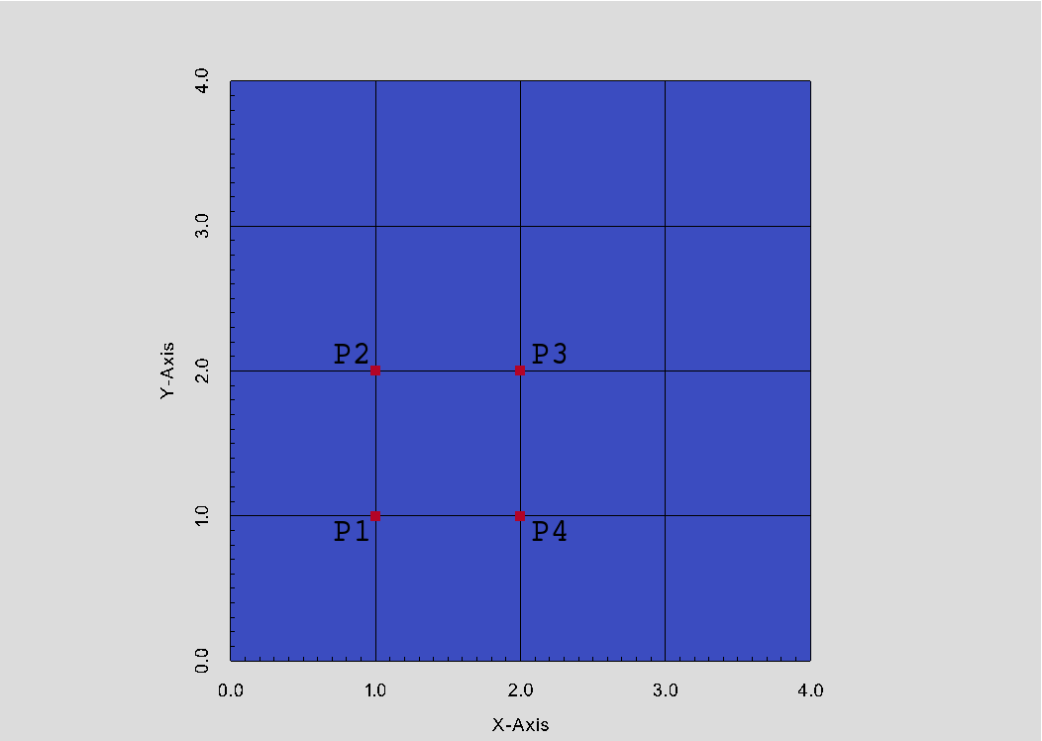

Figure 2: Position of the points for consideration of $\boldsymbol{U}$ and $\|E\|_F$.

6.2 Bending dominated plate deformation

For the second example we consider the midsurface $\boldsymbol{Y}(\eta^1, \eta^1) = [0, 1.5] \times [0, 1] \times 0$ of a plate with the thickness $h = 0.01875$. We approximate the midsurface by an initial mesh of 8×4 elements, shown in figure (3). Both boundaries in η^2-direction at $\eta^1 = 0$ and $\eta^1 = 1.5$, respectively, are hard clamped with inhomogeneous Dirichlet type boundary condtitions. We consider free bounding at the remaining edges.

For the left edge $(0, \eta^2, 0)^T$ we apply a prescribed displacement

$$\boldsymbol{U} = (0.75(1 - \cos t), \eta^2, 0.75 \sin t)^T$$

and for the right edge $(1.5, \eta^2, 0)^T$

$$\boldsymbol{U} = (-0.75(1 - \cos t), \eta^2, 0.75 \sin t)^T,$$

respectively, with $t \in \left[0, \frac{\pi}{2}\right]$. The outer normals of the edges will be rotated throughout their transport and are defined by

$$\frac{\partial \boldsymbol{U}}{\partial \boldsymbol{x}} = (\mp \cos t, 0, \sin t)^T, \text{ respectively.}$$

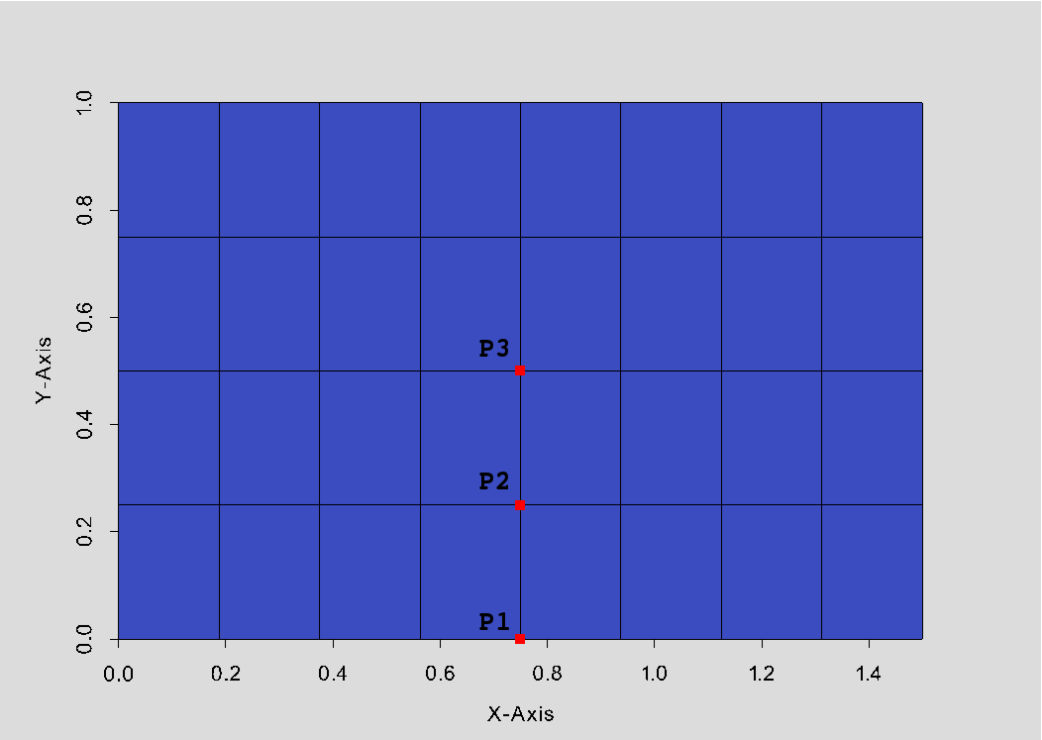

Figure 3: Initial mesh of the midsurface with the points for consideration of $\boldsymbol{U}$ and $\|E\|_F$.

The displacements are applied in 20 equidistant steps of t. Figure 4 shows the midsurface of the plate after these incremental steps, approximated with 32 elements (4a) and after further five refinement steps with $32,768$ elements (4b), respectively.

On every incremental step and every refinement step we use Newton's method with a stopping criterion $\varepsilon = 10^{-6}$.

The elements are coloured by the norm of the strain tensor. In the stage of 32 elements (4a), the maximum value is $5.0434e-02$ and after the refinements (figure 4b) we have a maximum value of $4.7635e-02$ of the strain. These values occur in the center of both free bounded edges. In contrast to the first example these values are very small.

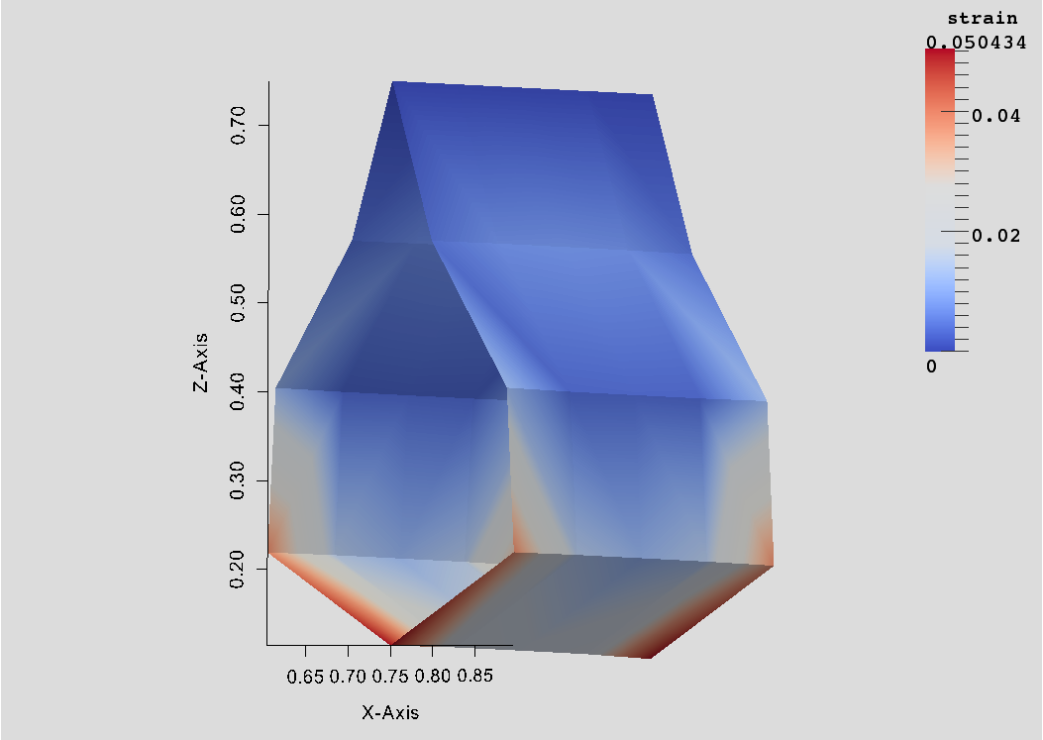

(a) 32 elements.

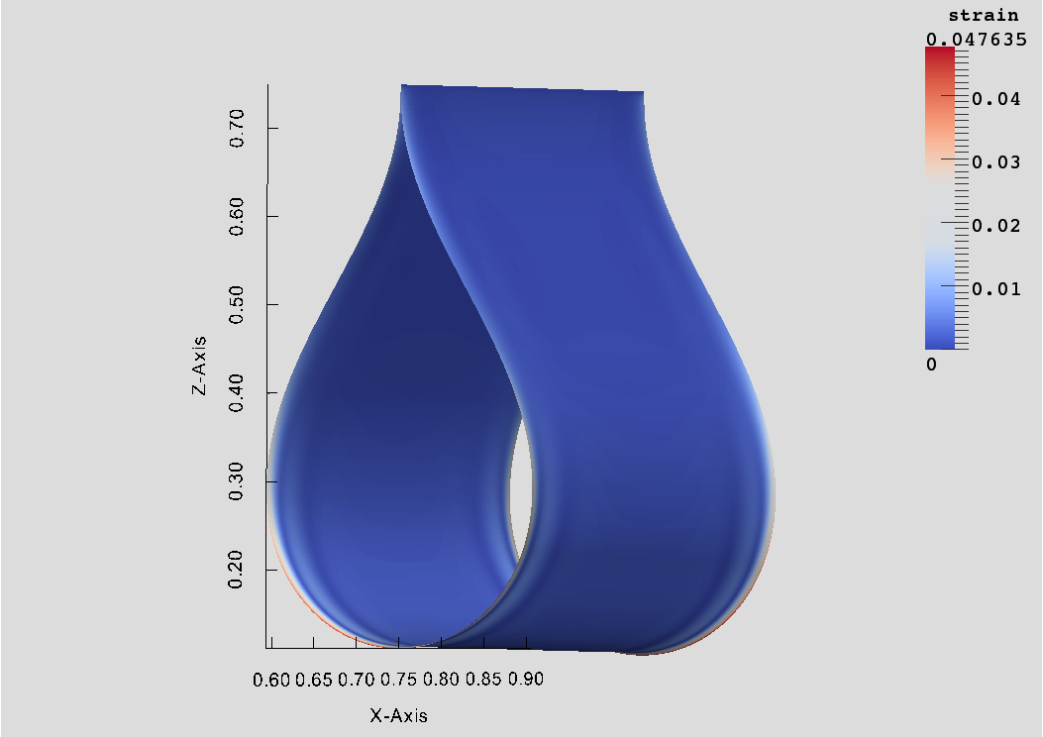

(b) 32768 elements.

Figure 4: Norm of the strain tensor at $\tau = 0$.

The average number of Newton steps during the stage of incrementation is about 5 and for the PCG iterations per Newton step about 59, respectively. In every mesh refinement we have 2 until 3 Newton steps and 265 PCG iterations per Newton step on average.

Figure 3 shows the considered points $P1(0.75, 0, 0)^T$, $P2(0.75, 0.25, 0)^T$ and $P3(0.75, 0.5, 0)^T$, in which we compare the components of the displacement vector $\boldsymbol{U}$ and the frobenius norm of the strain tensor $\|E\|_F$. Due to the symmetry of the example, we observed only the points on the lower half of the midsurface.

$\#El$		32	128	512	2048	8192	32768
$P1$	$U^{(1)}$	2.1E-05	-7.4E-07	-7.0E-07	-6.4E-07	6.2E-08	4.8E-08
	$U^{(2)}$	-3.9E-06	4.0E-05	1.9E-04	2.0E-04	2.0E-04	2.0E-04
	$U^{(3)}$	1.3E-01	1.1E-01	1.1E-01	1.1E-01	1.1E-01	1.1E-01
	$\|E\|_F$	4.4E-02	5.0E-02	4.6E-02	4.6E-02	4.7E-02	4.7E-02
$P2$	$U^{(1)}$	1.9E-05	-7.4E-05	-6.8E-07	-6.3E-07	6.2E-08	5.0E-08
	$U^{(2)}$	-3.7E-05	4.0E-05	1.9E-05	2.0E-05	2.0E-05	1.9E-05
	$U^{(3)}$	1.4E-01	1.2E-01	1.1E-01	1.1E-01	1.1E-01	1.1E-01
	$\|E\|_F$	1.6E-02	2.2E-02	4.9E-03	2.5E-03	2.5E-03	2.1E-03
$P3$	$U^{(1)}$	9.6E-06	-7.5E-07	-6.6E-07	6.4E-07	6.3E-08	5.1E-08
	$U^{(2)}$	-6.0E-06	-2.7E-08	-8.5E-09	-1.1E-09	-1.6E-10	-2.4E-09
	$U^{(3)}$	1.4E-01	1.2E-01	1.1E-01	1.1E-01	1.1E-01	1.1E-01
	$\|E\|_F$	1.2E-02	1.8E-02	5.1E-03	2.4E-03	2.3E-03	2.1E-03

Table 2: Displacement vector and the norm of the strain tensor in $P1$ until $P3$.

The comparison of the interesting values is seen in table 2 and shows that for all three points the first component of the displacement vector, $U^{(1)}$, is nearly zero.

For $P1$ and $P2$ we have a small value of the second component $U^{(2)}$. That means, that the plate shrinks in η^2-direction for a small value. This is the effect of the model of non linear elasticity. For $P3$, the midpoint of the midsurface, there is no displacement in direction η^2.

The $U^{(3)}$-component of the displacement vector is nearly the same at all three points.
The norm of the strain tensor increases from $P3$ to $P1$. Obviously the maximum of the norm is reached at the center of the free bounded edges.

References

[1] J.P. Boehler. *Applications of tensor functions in solid mechanics.* CISM Courses no 292, Springer, Wien, 1987.

[2] A.F. Bower. *Applied mechanics of solids.* CRC, Boca Raton, 2009.

[3] P.G. Ciarlet. *The Finite Element Method for Elliptic Problems.* North-Holland, Amsterdam, 1978.

[4] Arnd Meyer. Grundgleichungen und adaptive Finite-Elemente-Simulation bei Großen Deformationen. *Chemnitz Scientific Computing Preprints 07-02*, pages 1 – 8, 2002.

[5] Arnd Meyer. The koiter shell equation in a coordinate free description. *Chemnitz Scientific Computing Preprints 02-12*, pages 1 – 5, 2012.

Some titles in this CSC and the former SFB393 preprint series:

07-01 U. Baur, P. Benner. Gramian-Based Model Reduction for Data-Sparse Systems. February 2007.

07-02 A. Meyer. Grundgleichungen und adaptive Finite-Elemente-Simulation bei Großen Deformationen. Februar 2007.

07-03 P. Steinhorst. Rotationssymmetrie für piezoelektrische Probleme. Februar 2007.

07-04 S. Beuchler, T. Eibner, U. Langer. Primal and Dual Interface Concentrated Iterative Substructuring Methods. April 2007.

07-05 T. Hein, M. Meyer. Simultane Identifikation voneinander unabhängiger Materialparameter - numerische Studien. Juni 2007.

07-06 A. Bucher, U.-J. Görke, P. Steinhorst, R. Kreißig, A. Meyer. Ein Beitrag zur adaptiven gemischten Finite-Elemente-Formulierung der nahezu inkompressiblen Elastizität bei großen Verzerrungen. September 2007.

07-07 U.-J. Görke, A. Bucher, R. Kreißig Zur Numerik der inversen Aufgabe für gemischte (u/p) Formulierungen am Beispiel der nahezu inkompressiblen Elastizität bei großen Verzerrungen. October 2007.

07-08 A. Meyer, P. Steinhorst. Betrachtungen zur Spektraläquivalenz für das Schurkomplement im Bramble-Pasciak-CG bei piezoelektrischen Problemen. Oktober 2007.

07-09 T. Hein, M. Meyer. Identification of material parameters in linear elasticity - some numerical results. November 2007.

07-10 T. Hein. On solving implicitly defined inverse problems by SQP-approaches. December 2007.

08-01 P. Benner, M. Döhler, M. Pester, J. Saak. PLiCMR - Usage on CHiC. July 2008.

08-02 T. Eibner. A fast and efficient algorithm to compute BPX- and overlapping preconditioner for adaptive 3D-FEM. June 2008.

08-03 A. Meyer. Hierarchical Preconditioners and Adaptivity for Kirchhoff-Plates. September 2008.

08-04 U.-J. Görke, A. Bucher, R. Kreißig. Ein numerischer Vergleich alternativer Formulierungen des Materialmodells der anisotropen Elastoplastizität bei großen Verzerrungen. September 2008.

08-05 U.-J. Görke, R. Landgraf, R. Kreißig. Thermodynamisch konsistente Formulierung des gekoppelten Systems der Thermoelastoplastizität bei großen Verzerrungen auf der Basis eines Substrukturkonzepts. Oktober 2008.

08-06 M. Meyer, J. Müller. Identification of mechanical strains by measurements of a deformed electrical potential field. November 2008.

08-07 M. Striebel, J. Rommes. Model order reduction of nonlinear systems: status, open issues, and applications. November 2008.

08-08 P. Benner, C. Effenberger. A rational SHIRA method for the Hamiltonian eigenvalue problem. December 2008.

09-01 R. Unger. Obstacle Description with Radial Basis Functions for Contact Problems in Elasticity. January 2009.

09-02 U.-J. Görke, S. Kaiser, A. Bucher, R. Kreißig. A fast and efficient algorithm to compute BPX- and overlapping preconditioner for adaptive 3D-FEM. February 2009.

09-03 J. Glänzel. Kurzvorstellung der 3D-FEM Software SPC-PM3AdH-XX. January 2009.

09-04 P. Benner, Th. Mach. On the QR Decomposition of H-Matrices. July 2009.

09-05 M. Meyer. Parameter identification problems for elastic large deformations - Part I: Model and solution of the inverse problem. October 2009.

09-06 M. Meyer. Parameter identification problems for elastic large deformations - Part II: Numerical solution and results. November 2009.

09-07 P. Benner, S. Hein. Model predictive control based on an LQG design for time-varying linearizations. November 2009.

09-08 U. Baur, C. A. Beattie, P. Benner, S. Gugercin. Interpolatory Projection Methods for Parameterized Model Reduction. November 2009.

09-09 J. Saak, S. Schlömer. RRQR-MEX - Linux and Windows 32bit Matlab Mex-Files for the rank revealing QR factorization. December 2009.

09-10 M. Köhler, J. Saak. Efficiency improving implementation techniques for large scale matrix equation solvers. December 2009.

09-11 P. Benner, H. Faßbender. On the numerical solution of large-scale sparse discrete-time Riccati equations. December 2009.

10-01 A. Meyer, P. Steinhorst. Modellierung und Numerik wachsender Risse bei piezoelektrischem Material. May 2010.

10-02 M. Balg, A. Meyer. Numerische Simulation nahezu inkompressibler Materialien unter Verwendung von adaptiver, gemischter FEM. Juni 2010.

10-03 M. Weise, A. Meyer. Grundgleichungen für transversal isotropes Materialverhalten. Juli 2010.

10-04 M. K. Bernauer, R. Herzog. Optimal Control of the Classical Two-Phase Stefan Problem in Level Set Formulation. October 2010.

11-01 P. Benner, M.-S. Hossain, T. Stykel. Low-rank iterative methods of periodic projected Lyapunov equations and their application in model reduction of periodic

descriptor systems. February 2011.

11-02 G. Of, G. J. Rodin, O. Steinbach, M. Taus. Coupling Methods for Interior Penalty Discontinuous Galerkin Finite Element Methods and Boundary Element Methods. September 2011.

The complete list of CSC and SFB393 preprints is available via
`http://www.tu-chemnitz.de/mathematik/csc/`

Chemnitz Scientific Computing Preprints – ISSN 1864-0087